Journal of Neuroscience Methods 334 (2020) 108591

Contents lists available at ScienceDirect

Journal of Neuroscience Methods

journal homepage: www.elsevier.com/locate/jneumeth

Multiplex LA-ICP-MS bio-imaging of brain tissue of a parkinsonian mouse model stained with metal-coded affinity-tagged antibodies and coated with indium-spiked commercial inks as internal standards

Boris Neumann[a,b], Simone Hösl[b], Karima Schwab[a,*], Franz Theuring[a], Norbert Jakubowski[c]

[a] Charité – Universitätsmedizin Berlin, Corporate Member of Freie Universität Berlin, Humboldt-Universität Zu Berlin, and Berlin Institute of Health, Center for Cardiovascular Research, Institute of Pharmacology, Hessische Strasse 3-4, 10115 Berlin, Germany
[b] Proteome Factory AG, Magnusstrasse 11, 12489 Berlin, Germany
[c] Spetec GmbH, Berghamer Str. 2, 85435 Erding, Germany

ARTICLE INFO

Keywords:
LA-ICP-MS
Imaging
Internal standardization
Inkjet-Printing
DOTA-labelling immunohistochemistry
Parkinson's disease

ABSTRACT

Background: Immunohistochemistry techniques represent a powerful tool to detect and quantify disease related proteins. Improvements were accomplished by tagged antibodies using laser ablation and inductively coupled plasma mass spectrometry (LA-ICP-MS). However, these approaches are effected by day-to-variations due to instrumental drift.

New Method: Brain tissue from line 62, a Parkinson's disease model, and control mice were incubated with four antibodies relevant to the disease and standardized to three house-keeping proteins. In addition, a new standardization approach was developed and the results compared. This new approach consisted of coating specimens with gelatin and printing an indium-doped ink with a commercial ink jet printer. Furthermore, the method was evaluated for different ablation spot sizes with respect to resolution and signal-to-noise ratio.

Results: Normalization using house-keeping proteins led to high background signals even at high resolution. Normalization using indium-doped ink improved the signal-to-noise ratio even when small laser spot sizes were used and further improved by overlaying tissue specimen with gelatin.

Comparison with Existing Methods: Line 62 mice had more α-Synuclein and gliosis but decreased numbers of neurons, as found by conventional immunohistochemistry. These data are in line with the results obtained by LA-ICP-MS with indium standardization. However, differences between L62 and controls for tyrosine hydroxylase were only detected by LA-ICP-MS.

Conclusions: Internal standardisation using indium-doped inks is an effective method to overcome day-to-day variations and instrumental drifts. The new approach results in an increased signal-to-noise ratio and only under these conditions small but significant changes were detected, as seen for tyrosine hydroxylase.

1. Introduction

The first clinical immunoassay for detection of disease-related proteins using antigen-antibody-interactions was developed by Yalow and Berson in 1960s to quantify insulin in human blood (Yalow and Berson, 1996). For this technique, enzymes such as peroxidases were used to tag antibodies and, by addition of hydrogen peroxide as a substrate and tetramethylbenzidine as a chromogen, the reaction was photometrically detected. In the following years, such conjugates have been used during immunohistochemistry (IHC) investigations to target antigens directly in tissue samples, allowing the assessment of protein abundance at the cellular level (Grossman et al., 1998)

Later, IHC was combined with laser ablation inductively coupled plasma mass spectrometry (LA-ICP-MS) for element microscopy (Seuma et al., 2008). They used commercially available metal-tagged antibodies and a laser for ablating the whole tissue sample line by line. The

Abbreviations: DOTA, 1,4,7,10-tetraazacyclododecane-1,4,7,10-tetraacetic acid; DTPA, diethylenetriaminepentaacetic acid; GAPDH, glyceraldehyde 3-phosphate dehydrogenase; GFAP, glial fibrillary acidic protein; IHC, immunohistochemistry; LA-ICP-MS, laser ablation inductively coupled plasma mass spectrometry; MeCAT, metalcoded affinity tag; NeuN, neuronal nuclear antigen; Oxct1, Succinyl-CoA:3-ketoacid coenzyme A transferase 1; RSD, relative standard deviation; RT, room temperature; TH, tyrosine hydroxylase; α-Syn, α-synuclein

* Corresponding author.
E-mail address: karima.schwab@charite.de (K. Schwab).

https://doi.org/10.1016/j.jneumeth.2020.108591
Received 3 September 2019; Received in revised form 18 December 2019; Accepted 7 January 2020
Available online 08 January 2020

detected “mass fingerprints” of the multiple line scans were converted into two dimensional intensity profiles presenting the local distribution of the metal isotope and thus of the target protein. Imaging by LA-ICP-MS convinces with easy sample preparation, multi-elemental detection capabilities with high sensitivity and a spatial resolution in the micrometre range.

This first IHC approach from Seuma et al. (Seuma et al., 2008) was improved by Giesen et al. to a threefold multiplex using antibodies directed against three different biomarkers for breast cancer (Giesen et al., 2011). In 2014 and for the first time, Giesen et al. reached subcellular resolution (1 µm) for tissue samples in a multiplex immunoimaging approach using polymer tagged antibodies and LA-ICP-MS based on a time of flight instrument (Giesen et al., 2014). Thirty-two proteins and their modifications were simultaneously analysed in formalin-fixed paraffin-embedded human breast cancer sections and human mammary epithelial cells by use of metal-tagged antibodies (Giesen et al., 2014). Though feasibility of the LA-ICP-MS technology per se was well demonstrated, the study was limited however to samples derived from cancer tissue with well validated and highly abundant biomarkers, all of which with very high signal to noise ratio.

Various tagging methods for LA-ICP-MS were reported in literature (Giesen et al., 2012; Schwarz et al., 2014). For tagging chelates, macrocyclic compounds based on 1,4,7,10-tetraazacyclododecane-1,4,7,10-tetraacetic acid (DOTA) or linear chelates such as diethylenetriaminepentaacetic acid (DTPA) are used to strongly bind a metal, the latter is often a lanthanide element or one of its isotopes. Historically, chelating tagging compounds were first combined with radioactive tracers. McDevitt et al. presented a method for binding ^{225}Ac to a isothiocyanatobenzyl (SCN)-DOTA, and attached the complex to an IgG antibody (McDevitt et al., 2002). Soon after and for reasons related to safety, radioactive central ions were replaced by fluorescent lanthanides (e.g. Eu, Sm, Tb or Dy). The first immunoassay with ICP-MS and detection of metal labelled antibodies was introduced by the research group of Scott Tanner (Baranov et al., 2002). Later the technique was further improved by using polymer based lanthanide tags to increase sensitivity. Recently, Cruz-Alonso et al. used antibodies bio-conjugated with gold-nanoclusters which provide a high amplification factor in contrast to DOTA based labels (Cruz-Alonso et al., 2018).

Metal coding was first discussed by Whetstone et al. (Whetstone et al., 2004) while two years before Krause et al. (Krause et al., 2002) applied for a patent for a DOTA-based reagent with a cysteine reactive maleimide group with a biotin modification for purification and enrichment of tagged peptides via biotin-avidin affinity chromatography, named and patented as metal-coded affinity tag (MeCAT). Initially, tags containing only one detectable element atom per tag were used, but the sensitivity of ICP-MS was significantly increased through polymer tags (Lou et al., 2007).

To improve sensitivity, we have compared commercially available tagging reagents, such as polymer tags, SCN-DOTA and MeCAT. We found no high variations in sensitivity but a superior signal to noise (S/N) ratio for MeCAT (Waentig et al., 2012). Therefore, MeCAT was used in this investigation. A crucial point of LA-ICP-MS at a micrometre scale lies in the reduced laser spot size, which leads to a reduced ablated sample material and consequently to a severely decreased number of detectable atoms in the ablated area. Thus, a compromise between the number of tags per antibody and the size of the laser spot for ablation has to be found for every individual application. However, other factors such as total analysis time and analysis costs play an important role as well.

Noteworthy is also, that a valid normalisation is essential to overcome effects related to instrumental drift where high number of samples is ablated over a longer time period (Konz et al., 2012). Additionally, quantitative information can be gained if matrix matched calibration standards are applied (Wang et al., 2013). For internal standardisation and calibration in LA-ICP-MS, we have recently investigated a new approach using inks from commercial ink jet printer and, which are spiked with different elements (In, Th, Er and Pr). We have used this approach successfully on electroblot membranes (Hoesl et al., 2014) and tissue sections (Hoesl et al., 2016).

Therefore, it is the aim of this study to apply LA-ICP-MS in a multiplex mode using MeCAT tagged antibodies for simultaneous detection of proteins relevant to a disease. This approach is combined here with the concept of standardisation using metal-doped inks printed on top of the tissues, which will compensate for drift effects of the LA-ICP-MS instrument and guarantee day-to-day reproducibility. A conventional normalisation using housekeeping proteins such as ß-actin, GAPDH and OxcT1 (relatively quantified with MeCAT labelled antibodies) was used as a reference method.

As a model for Parkinson’s disease, we used brain tissue from h-α-SynL62 mice and their wild-type controls. These mice overexpress α-synuclein, which accumulates in different neuronal populations. Indeed, accumulation of α-synuclein in substantia nigra neurons and the consequent dopamine deficit is a hallmark of Parkinson’s disease, as these neurons seem highly susceptible to α-synuclein toxicity (Nieto et al., 2006). These neurons express the enzyme tyrosine hydroxylase (TH) to produce dopamine. Besides α-synuclein and TH, neuronal degeneration as well as inflammation have been associated with Parkinson’s disease (Gelders et al., 2018).

We applied a multiplex LA-ICP-MS imaging approach to measure some proteins relevant to our mouse model. We report the successful use of indium-doped inks as internal standard to substitute housekeeping proteins. This approach allows a more accurate comparison between larger sample cohorts and to detect minimal differences otherwise not detected using conventional IHC. Moreover, we have demonstrated the feasibility of multiplexing MeCAT-tagged antibodies, an important aspect in research areas with limited access to valuable samples, as it is the case for various neurodegenerative disorders.

2. Material and methods

2.1. Animals

Homozygous male and female α-synuclein transgenic mice (h-α-Syn L62, hereinafter termed L62) and C57BL6/J wild-type litters (WT), aged 7 months, were used in this study and were all naïve. Detailed characterisation of these mice can be found in Frahm et al. (Frahm et al., 2018). Transgenic mice overexpress full-length human α-synuclein, fused to a membrane-targeting N-terminal signal sequence, under control of the mouse *Thy1*-promoter. A total of twenty mice were group-caged and maintained in acclimatised holding rooms with a 12 h light/dark cycle (lights on at 6 a.m.) and with food and water *ad libitum*. Mice were euthanised in the morning by cervical dislocation; the top of the skull was exposed, and the overlying bone plates removed to allow harvest of the brain in an intact state. The right brain hemisphere was fixed overnight in neutral buffered formalin, embedded in paraffin and used for histological analysis. All animal experiments were performed in accordance with the European Communities Council Directive (2010/63/EU) and approved by the German Animal Research Ethics Committee of LAGESO (A0213/13). Ten mice per genotype with equal male/female numbers were used. The choice to include both genotypes is based on previous findings, where no gender differences were identified in terms of histopathology (Frahm et al., 2018).

2.2. Antibodies

Neuronal α-synuclein accumulation was relatively quantified with an antibody against α-Syn (Syn 204, Santa Cruz Biotechnology). Mature neurons were stained with an antibody against the neuronal nuclear antigen (NeuN, Clone A60, Merck Millipore), while an antibody against tyrosine hydroxylase (TH, H-196 Santa Cruz Biotechnology), the rate-limiting enzyme of dopamine synthesis, was used to relatively quantify dopaminergic neurons. As marker for inflammation, glial cells were

Table 1
Description of antibodies used for MeCAT labelling. AB: antibody, mAB: monoclonal antibody, pAB: polyclonal antibody.

Antigen	Antibody	Immunogen/ Epitope	Provider	Concentration AB [µg µL^{-1}]	Contaminants	Clean up	MeCAT-metal	Concentration AB-MeCAT [µg µL^{-1}]
α-Syn	Syn 204 (mAB)	human AA 95-109	SC Biotechnology (sc-32280)	1.0	0.1% gelatin	+	Eu	0.295
GFAP	Anti-GFAP (pAB)	cow spinal cord; not specified	Dako (# Z0334)	1.0	–	–	Ho	0.422
NeuN	Anti-NeuN (mAB)	mouse; not specified	Merck Millipore (Clone A60)	1.0	–	–	Pr	0.592
TH	Anti-TH (pAB)	human AA 1-196	SC Biotechnology (sc-14007)	1.0	0.1% gelatin	+	Tb	0.456
Oxct1	Anti-Oxct1 (pAB)	human AA 171-434	Abcam (ab105320)	1.0	–	–	Lu	0.825
ß-Actin	Anti-ß-Actin (mAB)	mouse; N-terminal	Sigma (A1978)	1.0	–	–	Nd	0.502
GAPDH	Anti-GAPDH (mAB)	Human full length	Abcam (ab9484)	1.0	–	–	Er	0.079

stained with an antibody against glial fibrillary acidic protein (GFAP, Dako). Antibodies against the housekeeping proteins ß-actin, glyceraldehyde 3-phosphate dehydrogenase (GAPDH) and Succinyl-CoA:3-ketoacid coenzyme A transferase 1 (OxcT1) were used as reference proteins for conventional normalisation.

Seven antibodies were tagged with MeCAT reagents (see Table 1) and used for antigen labelling of formalin-fixed paraffin-embedded brain sections as described below.

Conventional IHC experiments were conducted with unlabelled antibodies against α-Syn (Supplementary Table 2), TH (Supplementary Table 3), NeuN (Supplementary Table 4) or GFAP (Supplementary Table 5).

LA-ICP-MS imaging was performed with MeCAT-tagged antibodies. Experiments were run either in a single-plex manner (either α-Syn, TH, NeuN and GFAP, see Supplementary Tables 6–9 respectively), or in a multiplex manner, where each section was incubated with all seven antibodies at the same time (Syn 204, GFAP, NeuN, TH, ß-actin, GAPDH and Oxct1 altogether, see Supplementary Tables 10-13.

2.3. Clean up of antibodies formulated with gelatin

To remove excessive protein contamination of antibodies formulated with gelatin (see Table 1), a dedicated clean-up kit was used following the manufacturer's protocol (Pierce Antibody Clean-Up Kit, Cat# 44600, Thermo Scientific).

2.4. Lanthanide labelling of antibodies with MeCAT reagent

For MeCAT labelling, the method described earlier was used (Waentig et al., 2012). MeCAT loaded with the lanthanide of choice was prepared by Proteome Factory (Berlin, Germany). Reaction steps were performed in a centrifugal ultra-filtration device (30 kDa cut-off; Nanosep, VWR, Darmstadt, Germany). All reagents were dissolved in Tris buffer (20 mM Tris, 150 mM NaCl, 2.5 mM EDTA, pH 7). A molar excess rate of 600 of TCEP relative to antibody molarity was used for 30 min at 37 °C. For purification two washing steps using Tris buffer (see above) were conducted using ultra-filtration at 7,500 x *g* until hold-up volume was reached. After washing, the antibodies were tagged with the respective MeCAT-reagent with a 20-fold molar excess of MeCAT. The mixture was incubated for 60 min at 37 °C, followed by two washing steps using Tris buffer (see above) to purify the labelled antibody on the ultra-filtration membrane.

2.5. IHC and LA-ICP-MS imaging

Formalin-fixed, paraffin-embedded brain tissue was cut into 5 µm thin coronal sections (HM 325 Rotary Microtome, Thermo Scientific) at levels containing the substantia nigra, an area responsible for dopamine production and at Bregma 3.80 ± 0.25 mm, (Paxinos and Franklin, 2008). Duplicate consecutive sections for each animal and antibody were collected on SuperFrost® plus microscope glass slides (R. Langenbrinck GmbH, Germany), deparaffinised and used for IHC and LA-ICP-MS imaging. For IHC and single-plex- LA-ICP-MS ten mice per genotype and antibody were used (if not otherwise stated), while for multiplex experiments, six mice per genotype were used (see Table 2).

For IHC a method described earlier was used (Frahm et al., 2018). Briefly, sections were boiled in 10 mM citric buffer for antigen retrieval, incubated in 0.3% (v/v) hydrogen peroxidase solution and blocked for 20 min in blocking buffer (0.1% (w/v) BSA in PBS). Sections were then incubated either with antibodies Syn 204 (diluted 1:100), GFAP (diluted 1:500), NeuN (diluted 1:500) or TH (diluted 1:100) for 1 h at RT, followed by incubation with corresponding biotinylated secondary antibody (Dako, Denmark). Sections were developed with diaminobenzidine solution (Dako, Denmark), counterstained with Ehrlich haematoxylin solution (Carl Roth, Germany), embedded in Neo-Mount® (Merck Millipore, Germany) and images taken using a light microscope (Carl Zeiss, Jena, Germany). Those sections underwent conventional IHC evaluation. For this, immune-reactive signals for α-synuclein, NeuN or GFAP were quantified in relative manner for the whole right brain hemisphere without region specificity, while TH-positive dopaminergic neurons were counted in substantia nigra. Alpha-synuclein and TH positive neurons were counted manually, while NeuN and GFAP immunoreactivity was quantified as integrated density in 8-bit images using the ImageJ software (version 1.48v, NIH Image, National Institutes of Health, USA).

For single-plex (Syn 204, GFAP, NeuN or TH) and multiplex (Syn 204, GFAP, NeuN, TH, ß-actin, GAPDH and Oxct1) experiments, the antibodies (for details see Table 1) were applied for 1 h at RT, after antigen retrieval and blocking as described above. Syn 204 and TH were diluted 1:100, GFAP and NeuN were diluted 1:500, anti-ß-actin, anti-Oxct1 and anti-GAPDH were diluted to 0.5 µg/ml. Thereafter, the tissue was washed three times in 12 mM PBS buffer and air-dried overnight. After complete dryness, sections were coated with gelatin as described below.

2.6. Gelatin coating of microscope glass slides bearing brain tissue sections

To improve the efficacy of ablation and reduced in-between-sample variations, brain sections for LA-ICP-MS were treated with gelatin prior spiking of the internal standard. Treatment of glass slides with gelatin at different concentrations versus non-treated glass slides was evaluated during these pilot-experiments. Briefly, gelatin (Carl Roth, Karlsruhe) was dissolved in water, boiled and kept at 80 °C. SuperFrost® plus microscope glass slides with tissue sections were immersed into the hot

gelatin solution (either 2% or 5%) for about two seconds. After wiping the glass slide's bottom side and outer edges to remove excess gelatin solution, the slides were heated at 95 °C in horizontal position to allow the gelatin solution to completely dry. The gelatin coating procedure was conducted three times to guarantee an appropriate surface for printing of the standard solution. At this point the evenness of the gelatin layer itself was negligible since the ablation plane is identical to the plane of the internal standard application. Nevertheless, the thickness of the gelatin layers was measured as described below. Furthermore, the UV laser intensity was adjusted to completely ablate all of the UV-recipient organic material while leaving the glass slides blank.

To measure the thickness of the gelatin layer under final coating conditions, three glass slides without tissue sections were used. Three positions were marked on the glass slide and the thickness of each uncoated glass slide was determined using a 25 mm micrometer gauge (Carl Zeiss, Jena, Germany) for each of these three positions. Subsequently, the slides were coated five times with 5% gelatin solution as described above. After drying, the thickness at each of the three positions on each slide was measured. The coating procedure was repeated for additional 5 times (10 coating layers in total) and the thickness determined. The resulting 27 data points (3 positions on 3 glass slides and with 0, 5 and 10 coating layers) were plotted and to generate a standard curve for estimating the thickness of the gelatin.

2.7. Inkjet printer mediated spiking of indium as an internal standard

Indium-containing ink was used as internal standard and was printed on top of microscope glass slides (containing brain tissue sections) as previously described with some modifications (Hoesl et al., 2014). The standard was intentionally not spiked into the gelatin solution to circumvent variations of the standard concentration, which might emerge from unequal drying of the gelatin as observed for the edges of the glass slides.

In brief, the gelatin-coated glass slides were heated to 95 °C using a heat plate (Heidolph MR3100, Germany), transfered to the compact disc printing drawer (polystyrol, $t_m \approx 100$ °C) of a commercially available inkjet printer. The glass slides were printed three times with yellow ink spiked with 100 µg mL^{-1} indium (100 ppm). A relative printing density of 20% was selected in the printer settings dialog. Printing was performed in high-resolution mode (4800 dpi x 2400 dpi) with printing colour management disabled. In between printing cycles, the glass slides were incubated at 95 °C on the heat plate for rapid drying.

2.8. LA-ICP-MS imaging

A commercial LA system (NWR213, New Wave Portland, USA) with a beam expander and laser spot size between 4 µm and 250 µm, was attached to an ICP sector field mass spectrometer (Element XR, Thermo Fisher Scientific, Germany). The ICP-MS was synchronised with the LA unit in an external trigger mode. The slides with the brain tissue sections, coated with gelatin and spiked with indium-containing ink, were placed in the sample holder and inserted into a two-volume cell (NWR213). Ablation was conducted in a differential line scan mode with an approximate overlap of 10% in laser ablation areas to its preceding line as described by Giesen et al. (Giesen et al., 2014).

The aerosol was transported by helium at a flow rate of 1 L min^{-1} and argon was added at a typical flow rate of 0.8 L min^{-1} in front of the ICP torch. The LA-ICP-MS was tuned daily for maximum ion intensity and low oxide ratio (ThO/Th ratio < 3%) and a relative standard deviation (RSD) for thorium ≤ 5%. The tuning was conducted on a microscopic glass slide. Samples were completely ablated line by line under optimised LA-ICP-MS conditions (0.20-0.25 mJ) as summarised in supplementary Table 1. The following isotopes were selected: ^{113}In, ^{141}Pr, ^{146}Nd, ^{153}Eu, ^{159}Tb, ^{165}Ho, ^{166}Er, ^{175}Lu.

For analysis of the tissue sections, spot sizes of 35 and 130 µm and scan speeds of 50 and 150 µm s^{-1} were used, respectively.

The LA-ICP-MS data were imported to Origin 8 (Origin lab Corporations, Northampton, USA) where intensity time profiles or color-coded images were produced by transforming the scan time into a micrometre scale. Signal intensities were colour coded in a way that low intensities are shown in blue and high intensities in red colour. The data normalisation was performed in Excel (Microsoft, Redmond, USA) by multiplication of each lanthanide data point with an individual normalisation factor derived from the indium signal:

$$I_{norm.}^{Lanthanide} = I^{Lanthanide} * \frac{I_{mean}^{Indium}}{I^{Indium}}$$

For quality assessment, the ICP-MS instrumentation was optimised weekly using a micro mist nebuliser and a liquid standard in a cyclone spray chamber (Glass Expansion, Melbourne, Australia) at a transport gas rate of 1 L min^{-1}. The settings for the ion lenses and the high frequency power were optimised with a tune standard solution containing sodium, indium and uranium at a concentration of one ng mL^{-1}. All optimisation steps were carried out at a low-resolution setting of R = 300 at a sample uptake rate of 1 mL min^{-1}. Minimal signal parameters for the optimisation were chosen as follow: 1.2×10^6 cps for indium and 1.8×10^6 for the uranium signal at a RSD < 2%. Additionally, for the LA-ICP-MS analysis, an optimisation of the gas flows, the plasma torch position and the ion lenses settings were conducted daily. Conventional nickel cones were used for the interface regions of LA-ICP-MS instrument (Element XR, Thermo Fisher Scientific, Bremen, Germany). For comparison with the results from IHC, all measured samples were normalised, and background corrected intensities were integrated for the whole brain section.

2.9. Data analyses

Data for IHC and LA-ICP-MS were expressed as group mean and standard error (S.E). Statistical analyses were conducted with GraphPad Prism (version 6.00; GraphPad Software Inc., La Jolla, CA, USA), using unpaired t-test. The null hypothesis was accepted for $\alpha < 0.05$ and only significant terms are given in the text.

3. Results and discussion

3.1. Study design

Within this study, the abundance of four Parkinson's disease-related proteins was analysed in brain tissue of L62 α-synuclein transgenic mice using LA-ICP-MS imaging and IHC. These mice overexpress human α-synuclein under control of the *Thy-1*-promoter and are characterised by accumulation of α-synuclein in different neuronal populations, neuronal degeneration and progressive motor deficits (Frahm et al., 2018). Further, these mice exhibit dopamine depletion without frank loss of TH-positive, dopamine-producing neurons of the substantia nigra, the main source of dopamine (Frahm et al., 2018). It has been shown before that L62 released less dopamine under pharmacological stimulation. Nevertheless, no changes in the number of dopamine-producing, TH-positive cells was found using IHC, nor in the abundance of TH as found by electroblotting (Frahm et al., 2018). In addition, L62 mice exerted some gliosis, evident as elevated number of GFAP-positive neurons in multiple brain areas, such as the cortex, the hippocampus and the substantia nigra (data not shown). In focus of this work were therefore the four proteins α-Syn, TH, NeuN and GFAP. Brain sections from L62 (n = 10) and their WT controls (n = 10) were used to access the relative protein abundance. Each group had identical distribution of gender (5 female (f) and 5 male (m)). Furthermore, for each animal two adjacent sections were prepared (two technical replicates).

To evaluate the robustness of LA-ICP-MS imaging, a parallel approach with conventional IHC was performed using replicate brain sections. In deviation to conventional IHC staining, primary antibodies

used here were tagged with MeCAT.

An obvious reason for superiority of LA-ICP-MS over IHC is that LA-ICP-MS imaging can be operated in a multiplex mode. Theoretically, for lanthanide elements a 32-plex mode is possible, using enriched isotopes. However, some isotopes can have interferences with other lanthanide elements and should be selected accordingly. In general, IHC is mostly operated in a single-plex manner, except for immunofluorescence, where three antibodies can be applied simultaneously. Further, IHC is based on peroxidase-tagged antibodies with 3,3′-Diaminobenzidine as a substrate and is not an endpoint reaction. Consequently, and because any standardisation is lacking, day-to-day or lab-to-lab variations cannot be excluded. Consequently, study cohorts need to undergo the IHC procedure at the exact same time, which is not convenient for large cohorts. On the contrary, such variations can be well managed during LA-ICP-MS simply by introducing internal standards. One approach to address this standardisation issue for LA-ICP-MS imaging examinations is either using different housekeeping proteins or spiked internal standards, and both will be discussed below.

3.2. Internal standardisation using housekeeping proteins

To correct for instrument drift, minimise background noise and to compensate for small variations of tissue section thickness, internal standardisation using different housekeeping proteins was applied. For this, the respective signals for the four Parkinson's disease-related antibodies directed against the proteins α-Syn (^{153}Eu), TH (^{159}Tb), NeuN (^{141}Pr) and GFAP (^{165}Ho) were extracted from the acquired data and normalised to the signals of the three antibodies directed against the housekeeping proteins GAPDH(^{166}Er), Oxct1 (^{175}Lu) and β-Actin (^{146}Nd). Those normalised values were used to generate 2D-intensity profiles and representative images are shown in Fig. 1.

As shown in the Fig. 1 normalisation using each of three housekeeping proteins resulted in obviously different images. While the Oxct1-normalised signal shows low background for the four proteins of interest, it also lowers the contrast for positive areas (e.g. TH^{159}Tb/^{175}Lu). On the other hand, β-Actin normalisation provides satisfactory results for α-Syn (^{153}Eu), as it results in a homogenous distribution, but fails for GFAP (^{165}Ho/^{146}Nd) where it enhances the area of false positive staining. Moreover, normalisation via housekeeping proteins leads to high background signals, when data were acquired at higher resolution using 35 µm (data not shown). Mixed effects were observed for all three housekeeping protein mediated normalisation approaches. For some antigens, they enhanced the contrast or minimised the background but there was no obvious improvement of the data. Overall, the distribution of the selected housekeeping proteins is too heterologous to be recommended to act as a reference for internal standardisation. However, it appears that housekeeping protein related normalisation could be useful in selected limited cases only.

3.3. Internal Standardisation using inkjet printer spiked indium as internal standard

As an alternative for internal standardisation during LA-ICP-MS examination, ink jet printing of metal containing inks were already applied to overcome instrumental drift effects of the laser ablation and ICP-MS system. We have recently published an approach using ink spiked with different elements, such as In, Th, Er and Pr. The ink was applied to samples with a commercial ink jet printer and this was successfully used on electro blot membranes (Hoesl et al., 2014) and tissue sections (Hoesl et al., 2016; Moraleja et al., 2018, 2016). This approach will be used here to overcome also day-to-day variations, which is a prerequisite for a long-term study.

Microscope glass slides have an individual surface character, which may cause inhomogeneity during application of hydrophilic ink formulations for standardisation. For example, we observed that in some areas the ink might roll off the surface and accumulate in certain droplet clusters. To overcome this obstacle, empty glass slides (with no brain tissue sections) were coated with a layer of gelatin (Moraleja et al., 2016). Gelatin was applied at two different concentrations of either 2% or 5%. The homogeneity of the printed indium-spiked ink application was evaluated using two different laser spot sizes for the ablation (130 µm vs. 35 µm). Random areas within the printed areas of the glass slides were ablated and with LA-ICP-MS. The resulting signal heights, as well as absolute and relative standard deviations (SD and RSD) were extracted or calculated respectively and plotted. The false-colour heat-maps for the acquired data of around 3 mm x 5 mm area are given in Fig. 2.

Application of internal standard onto uncoated sample slides resulted in inhomogeneity, which is reflected by the insufficient RSD value (44%, see Fig. 2). The RSD was improved to 27% through coating with 2% gelatin and using a spot size of 130 µm. The improvement was ameliorated when the gelatin concentration was increased to 5% (8 % RSD). The enhancement of the homogeneity mediated by the treatment with 5% gelatin solution was also observed using a laser spot size of 35 µm (RSD 14%).

In summary, these experiments revealed that gelatin coating greatly enhances the homogeneity of the internal standard distribution (^{115}In) applied by inkjet printing. Therefore, all following LA-ICP-MS imaging experiments were done using 5% gelatin for brain tissue coating followed by indium printing and all intensity measurements were normalised to this isotope. The gelatine layer had a thickness of 6.47 ± 0.62 µm (data not shown).

3.4. Effect of laser spot size on image resolution and quality

Obvious from the heat map figure from the gelatin experiments described above (Fig. 2), the resolution of the measurement is significantly dependent on the laser spot size. During LA-ICP-MS imaging, a huge amount of data is being acquired, with to date no software available for automatic data evaluation and construction of the surface plots. Thus, a compromise between resolution and time consumption must be found.

Using the sections designed for LA-ICP-MS imaging and after antibody application (α-Syn (^{153}Eu), TH (^{159}Tb), NeuN (^{141}Pr) and GFAP (^{165}Ho)), gelatin coating (5%) and indium-spiking (^{115}In), sections were ablated with laser spot sizes of either 130 µm or 35 µm. Velocity of the laser was changed to match the spot size, as given in the figure legends (Fig. 3 and Fig. 4). For the 130 µm, spot size we used a laser scanning velocity of 150 µm s^{-1} and for the 35 µm spot size a velocity of 50 µm s^{-1} was used.

A characteristic distribution for the four proteins of interest was detected with either spot size. This is obvious from comparison with the IHC results obtained in this work (see micrograph in Fig. 5) and, which are in line with previously published data (Frahm et al., 2018). Though reducing the spot size from 130 µm to 35 µm decreased the amount of ablated sample and consequently of the measured signal, nevertheless the signal intensity obtained with 35 µm had enough signal to noise ratio. As expected, the resolution and the contrast of the pictures obtained was enhanced with the lower size of the laser spot (compare Fig. 3 for 130 µm and Fig. 4 for 35 µm), as the pictures obtained with 35 µm spot size seem less blurry. Apparent is also that the difference in local protein distribution is quite large, and this was much less appreciated from staining derived from IHC. From this data, it is obvious that the dynamic range is one of the main differences between LA-ICP-MS imaging and IHC and this have been well reviewed (Bodenmiller, 2016).

As stated above, a higher local resolution is achieved using a smaller spot size but the total analysis time for each sample is increased to 8 h, whereas for the spot size of 130 µm only 3 h are needed. For this reason, six samples were selected for measurements with the higher local resolution, to demonstrate the high quality of the multiplex measurements, but for data analysis and for comparison with the IHC all

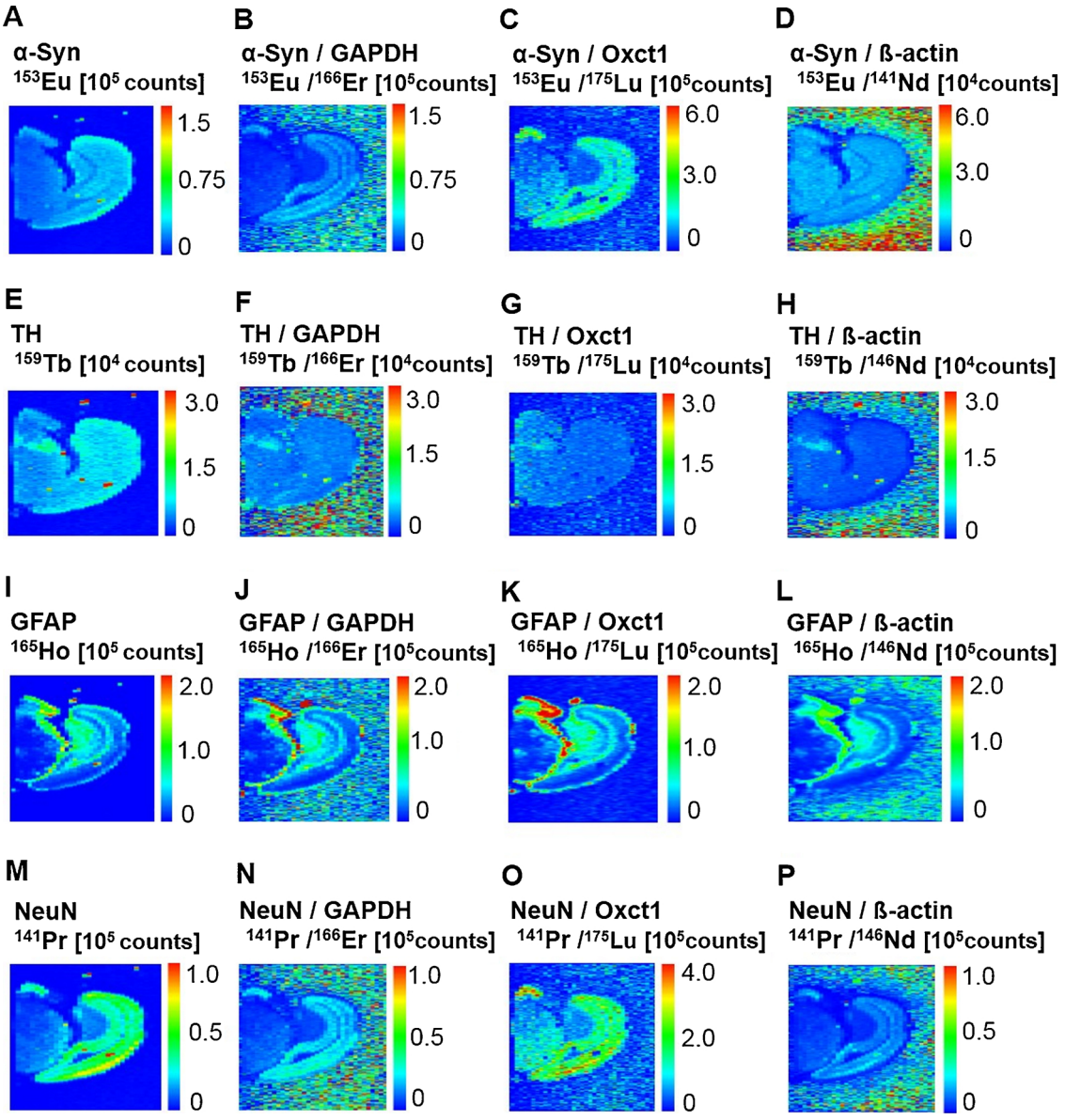

Fig. 1. The effect of normalisation based on housekeeping proteins. Representative intensity images for the four proteins α-Syn (A–D), TH (E–H), GFAP (I–L) and NeuN (M–P) with and without housekeeping protein-based normalisation. The ablation was conducted using a laser spot size of 130 µm. The intensity profiles without normalisation are shown for α-Syn (A), TH (E), GFAP (I) and NeuN (M). Three different housekeeping proteins were used for normalisation: GAPDH (B for α-Syn, F for TH, J for GFAP and N for NeuN), Oxct1 (C for α-Syn, G for TH, K for GFAP and O for NeuN) and ß-actin (D for α-Syn, H for TH, L for GFAP and P for NeuN). All antibodies used were labelled with MeCAT-lanthanides: anti-α-Syn-MeCAT(^{153}Eu), anti-TH-MeCAT(^{159}Tb), anti-GFAP-MeCAT(^{165}Ho), anti-NeuN-MeCAT(^{141}Pr), anti-GAPDH-MeCAT (^{166}Er), anti-Oxct1-MeCAT(^{175}Lu) and anti-β-actin-MeCAT(^{146}Nd).

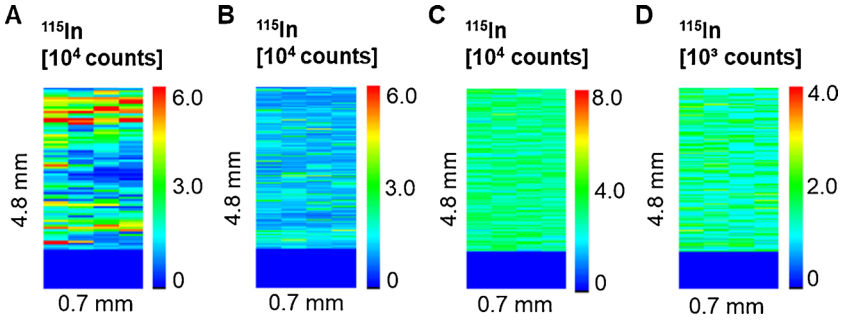

Fig. 2. The effect of gelatin-coating on ablation of the internal standard ^{115}In. Representative intensity images zoomed for illustration of ^{115}In-spiked glass slides non-coated (A) and coated with 2% gelatin (B) or 5 % gelatin (C) and ablated with a laser spot size of 130 µm (A–C) or 35 µm (D). The internal standard ^{115}In was applied using a commercial inkjet printer.

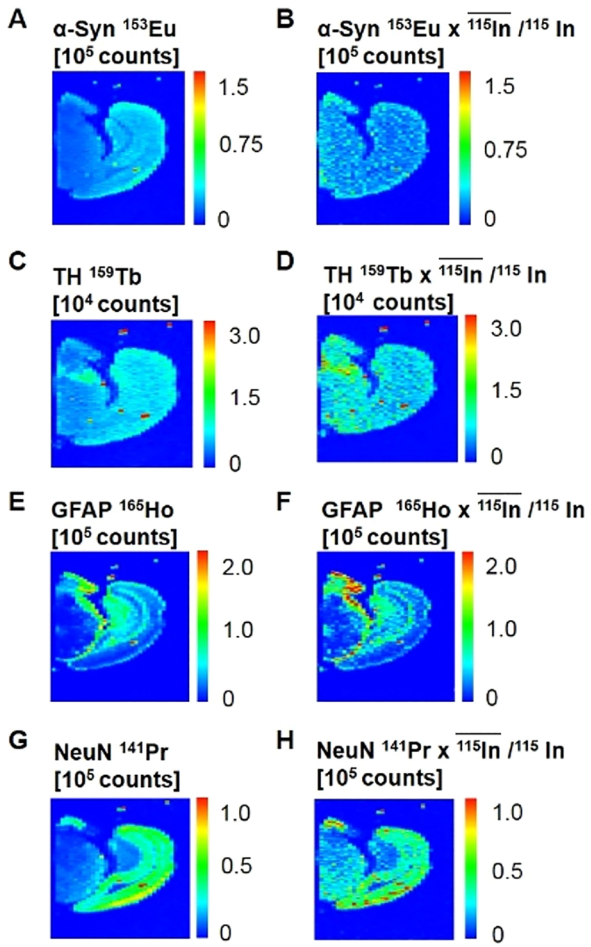

Fig. 3. Normalisation of α-Syn, TH, GFAP and NeuN using ^{115}In as a standard and a large laser size for ablation. Representative midbrain image plots from sections tagged with antibodies against α-Syn (A and B), TH (C and D), GFAP (E and F) and NeuN (G and H) using no normalisation (A, C, E and G) or normalisation with the internal standard ^{115}In (B, D, F and H). The internal standard ^{115}In was applied on top of the brain sections using an inkjet printer. Samples were ablated with a laser spot size of 130 µm and analysed by ICP-MS. All antibodies used were labelled with MeCAT-lanthanides: anti-α-Syn-MeCAT(^{153}Eu), anti-TH-MeCAT(^{159}Tb), anti-GFAP-MeCAT(^{165}Ho), anti-NeuN-MeCAT(^{141}Pr). All data were acquired with simplex LA-ICP-MS.

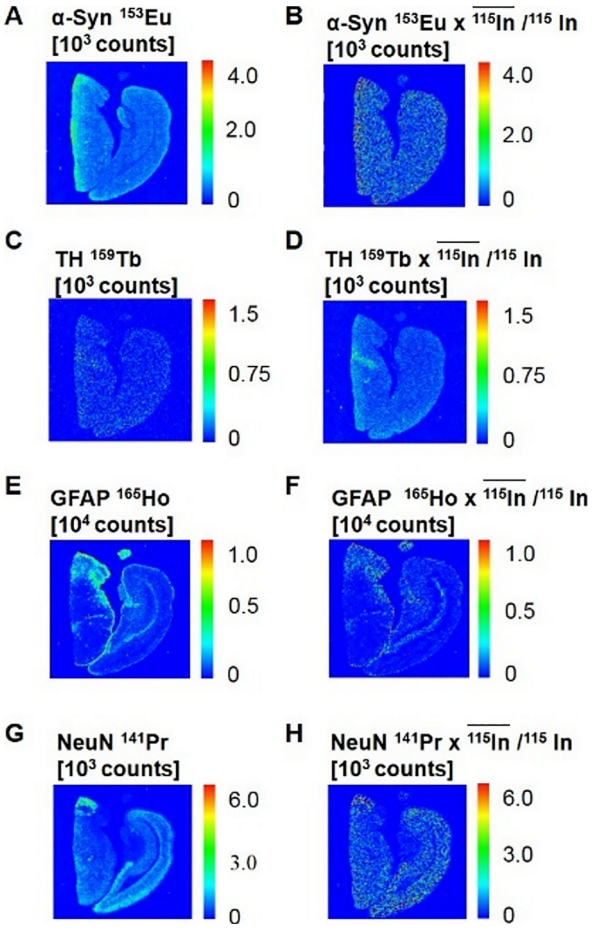

Fig. 4. Normalisation of α-Syn, TH, GFAP and NeuN using ^{115}In as a standard and a small laser size for ablation. Representative midbrain image plots with antibodies against α-Syn (A and B), TH (C and D), GFAP (E and F) and NeuN (G and H) using no normalisation (A, C, E and G) or normalisation with the internal standard ^{115}In (B, D, F and H). The internal standard ^{115}In was applied on top of the brain section using an inkjet printer. Samples were ablated with a laser spot size of 35 µm and analysed by ICP-MS. All antibodies used were labelled with MeCAT-lanthanides: anti-α-Syn-MeCAT(^{153}Eu), anti-TH-MeCAT(^{159}Tb), anti-GFAP-MeCAT(^{165}Ho), anti-NeuN-MeCAT(^{141}Pr). All data were acquired with simplex LA-ICP-MS.

information were gained with the lower resolution of 130 µm only. The integrated raw data were normalised to the respective ^{115}In signals acquired at identical location.

3.5. Critical review of IHC and LA-ICP-MS imaging

As stated above, L62 mice were presented with accumulation of α-Syn (increased number of α-Syn-positive neurons), neuronal degeneration (decreased number of NeuN-positive neurons), gliosis (increased number of GFAP-positive neurons), as well as a hypodopaminergic state. Though we were not able to measure any changes related to TH, neither with IHC (current work and (Frahm et al., 2018)), not electro blotting (Frahm et al., 2018), the dopaminergic phenotype was evident from pharmacological studies and was highly significant (Frahm et al., 2018). During the current work, we aimed to relatively quantify the four above-mentioned proteins using single-plex and multiplex-LA-ICP-MS. Those results were further compared and validated with conventional IHC.

Representative IHC micrographs for WT and L62 mice are shown in Fig. 5(A–D for WT and E–H for L62). During IHC examinations, α-Syn-positive and TH-positive neurons were counted manually, while GFAP and NeuN relative immunoreactivity signals were quantified as integrated density using the ImageJ tool. As shown in Fig. 5, L62 mice exhibited a significantly higher number of α-Syn-positive neurons ($p < 0.0001$, Fig. 5I), while no differences in TH-positive neurons were seen (Fig. 5J), when compared to WT. Relative to WT, GFAP-immunoreactivity significantly increased ($p = 0.0043$, Fig. 5K) and NeuN-immunoreactivity was significantly decrease ($p < 0.0001$, Fig. 5L) in L62 mice. All those observations are in line with data reported before (Frahm et al., 2018).

Relative quantification for single-plex LA-ICP-MS derived plots revealed very similar results for α-Syn ($p < 0.0001$, Fig. 6A), GFAP ($p < 0.0001$, Fig. 6C) and NeuN ($p < 0.0001$, Fig. 6D), but the statistical power for the GFAP results obtained by LA-ICP-MS imaging was superior to that obtained by IHC. As for TH, examination with LA-ICP-MS revealed a subtle but a statistically highly significant relative decrease of TH-signal in L62 compared to WT ($p = 0.009$, Fig. 6B). This agrees with the pharmacologically measured hypodopaminergic state and reveals clearly that this extra information could be obtained by LA-ICP-MS imaging only. The discrepancy for TH results derived from LA-ICP-MS and IHC might be related to higher dynamic range offered by LA-ICP-MS and, which is enhanced by internal standardisation. In summary, we found for LA-ICP-MS imaging a higher dynamic range and

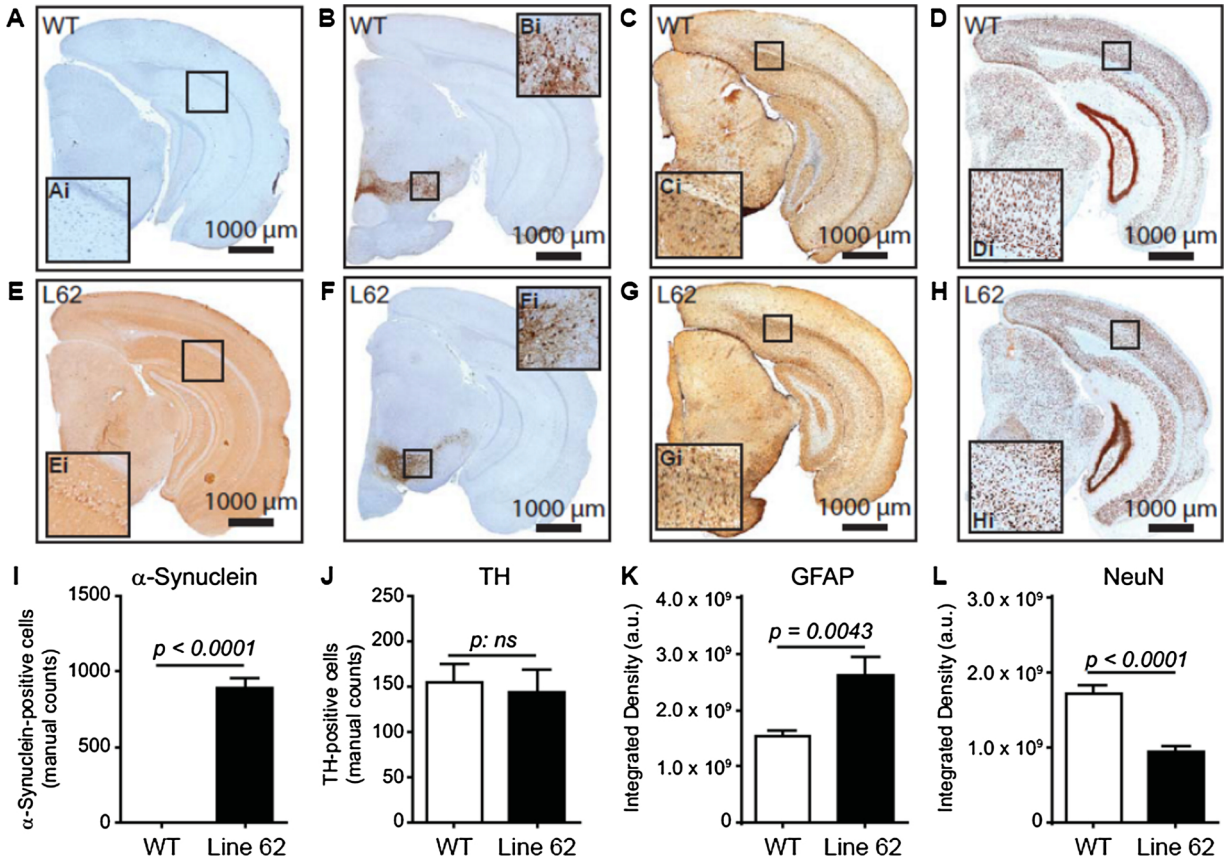

Fig. 5. Quantification of α-Syn, TH, GFAP and NeuN using IHC. Representative micrographs from midbrain of WT (A–D) and L62 (E–H) brain sections stained with antibodies against α-Syn (A and E), TH (B and F), GFAP (C and G) and NeuN (D and H) using conventional IHC. Immuno-reactive signals for α-Syn, NeuN and GFAP were relatively quantified in the whole right brain hemisphere without region specificity, while TH-positive dopaminergic neurons were counted in substantia nigra, the only immune-reactive region in the brain area analysed. Alpha-Syn and TH positive neurons were counted manually, while NeuN and GFAP immune-reactivity was quantified relatively as integrated density using the ImageJ software. Two sections per mouse and antibody were analysed and the mean value over sections for each mouse was calculated and used for analyses. Quantitative values are shown as group mean + S.E. for α-Syn (I), TH (J), GFAP (K) and NeuN (L). Statistical analysis was conducted with unpaired t-test. N = 6–10 for WT and 9–10 for L62 per antibody. For more details on cohorts, see Supplementary Tables.2–5.

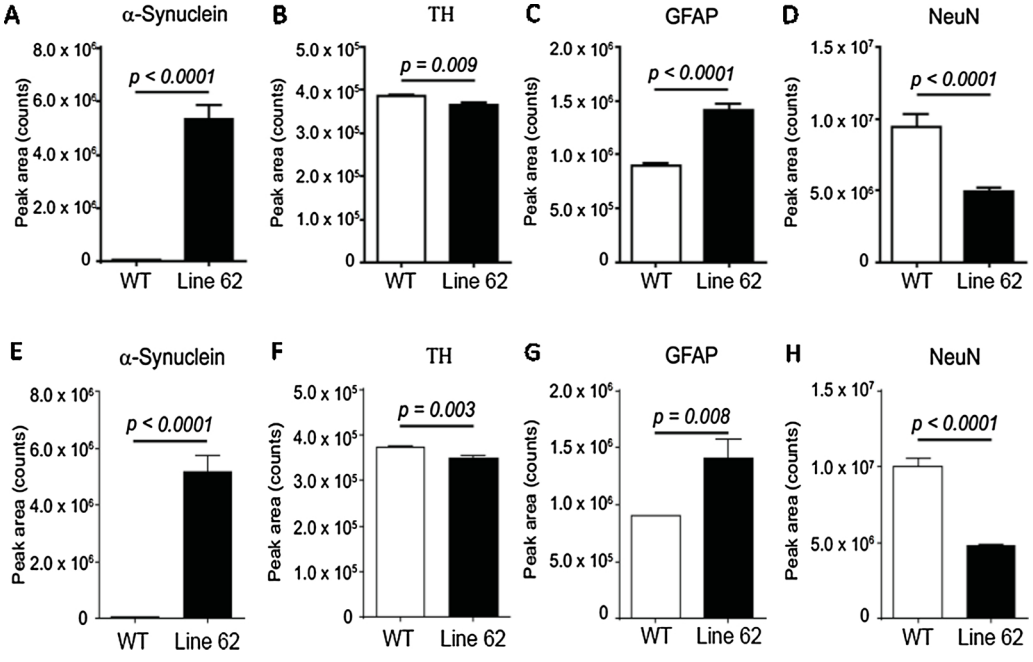

Fig. 6. Relative quantification of α-Syn, TH, GFAP and NeuN using single-plex LA-ICP-MS (A–D) and multiplex- LA-ICP-MS (E–H). Proteins from brain sections of WT and L62 were detected using MeCAT-tagged antibodies against α-Syn (A and E), TH (B and F), GFAP (C and G) and NeuN (D and H) and spiked with the internal standard ^{115}In using an inkjet printer. Samples were ablated with a laser spot size of 130 µm and analysed by ICP-MS. All antibodies used were tagged with MeCAT-lanthanides: anti-α-Syn-MeCAT(^{153}Eu), anti-TH-MeCAT(^{159}Tb), anti-GFAP-MeCAT(^{165}Ho), anti-NeuN-MeCAT(^{141}Pr). For each antibody, the acquired values were normalised to the internal standard ^{115}In. Two sections per mouse and antibody were analysed and the mean value over sections for each mouse was calculated and used for analyses. Semi-quantitative values are shown as group mean + S.E. for α-Syn (A and E), TH (B and F), GFAP (C and G) and NeuN (D and H). Statistical analysis was conducted with unpaired t-test. N = 5–9 for WT and 4–10 for L62 per antibody. For more details on cohorts and their respective size, see Supplementary Tables 6–9 for single-plex and 10–14 for multiplex LA-ICP-MS.

higher sensitivity compared to IHC, which allowed unravelling small changes, otherwise not detectable. Furthermore, the specificity of the four antibodies used here was not compromised by the lanthanide-MeCAT labelling procedure and was preserved during multiplex experiments, where we applied seven antibodies simultaneously (Fig. 6E–H). As obvious from bar graphs, multiplex-LA-ICP-MS revealed similar results as the single-plex experiments: α-Syn-positive neurons were increased in L62 compared to WT mice ($p < 0.0001$, Fig. 6E), TH-positive neurons were decreased in L62 mice ($p = 0.003$ Fig. 6F), GFAP-immunoreactivity was significantly increased ($p = 0.008$, Fig. 6G) and NeuN-immunoreactivity significantly decreased ($p < 0.0001$, Fig. 6H) in L62 mice relative to WT. Thus, for the tagging conditions used here our results are not limited by molecular hindering or loss of specificity.

4. Conclusion

Collectively, we have shown that the internal standardisation using indium-doped inks printed onto samples by a commercial printer is an effective method to overcome day-to-day variations and instrumental drifts. The distribution of the standard was further improved by coating the samples by gelatin. This relatively simple approach was a prerequisite for a long-term large cohort study. It could be used to overcome in-between lab variations if applied together with known reference material. Further, we have shown the feasibility of multiplexing MeCAT-tagged antibodies without compromising antibody specificity in an imaging approach using LA-ICP-MS. This study was limited to seven isotopes but only by the relatively slower scanning ability of our ICP-MS instrument. Theoretically, this number can reach 40 isotopes (Wang et al., 2013) if fast scanning CyTOF-MS is coupled to a novel laser ablation system with much shorter wash out times. Thus, the higher laser repetition rates and faster laser scanning conditions could be used in future studies to reduce analysis time or alternatively to use a higher lateral resolution.

Author contributions

BN, SH and KS designed and performed experiments and analysed the data; KS performed statistical analyses; BN, KS and NJ conceived the project and wrote the paper and all authors read and reviewed the final manuscript.

Funding

SH received financial support by the “Bundesministerium fuer Wirtschaft und Energie, Projektnummer MNPQ 09/10″.

Declaration of Competing Interest

BN and SH were employed by Proteome Factory AG. NJ was employed by Spetec GmbH. The other authors declare that the research was conducted in the absence of any commercial or financial relationships that could be construed as a potential conflict of interest.

Acknowledgments

The authors acknowledge Mandy Magbagbeolu for the technical support with brain tissue sectioning and immunohistological staining. We also thank Prof. Christian Scheler for his support of this study. The MS-data was acquired at Bundesanstalt für Materialforschung und -prüfung (BAM), Richard-Willstaetter-Strasse 11, 12,489 Berlin, Germany in the former research group of Nobert Jakubowski (retired). We thank TauRx Therapeutics Ltd. (Singapore) for their permission to use the L62 mice.

Appendix A. Supplementary data

Supplementary material related to this article can be found, in the online version, at doi:https://doi.org/10.1016/j.jneumeth.2020.108591.

References

Baranov, V.I., Quinn, Z., Bandura, D.R., Tanner, S.D., 2002. A sensitive and quantitative element-tagged immunoassay with ICPMS detection. Anal. Chem. 74, 1629–1636. https://doi.org/10.1021/ac0110350.

Bodenmiller, B., 2016. Multiplexed epitope-based tissue imaging for discovery and healthcare applications. Cell Syst. 2, 225–238. https://doi.org/10.1016/J.CELS.2016.03.008.

Cruz-Alonso, M., Fernandez, B., García, M., González-Iglesias, H., Pereiro, R., 2018. Quantitative imaging of specific proteins in the human retina by laser ablation ICPMS using bioconjugated metal nanoclusters as labels. Anal. Chem. 90, 12145–12151. https://doi.org/10.1021/acs.analchem.8b03124.

Frahm, S., Melis, V., Horsley, D., Rickard, J.E., Riedel, G., Fadda, P., Scherma, M., Harrington, C.R., Wischik, C.M., Theuring, F., Schwab, K., 2018. Alpha-Synuclein transgenic mice, h-α-SynL62, display α-Syn aggregation and a dopaminergic phenotype reminiscent of Parkinson’s disease. Behav. Brain Res. 339, 153–168. https://doi.org/10.1016/j.bbr.2017.11.025.

Gelders, G., Baekelandt, V., Van der Perren, A., 2018. Linking neuroinflammation and neurodegeneration in parkinson’s disease. J. Immunol. Res. 2018, 1–12. https://doi.org/10.1155/2018/4784268.

Giesen, C., Mairinger, T., Khoury, L., Waentig, L., Jakubowski, N., Panne, U., 2011. Multiplexed immunohistochemical detection of tumor markers in breast cancer tissue using laser ablation inductively coupled plasma mass spectrometry. Anal. Chem. 83, 8177–8183. https://doi.org/10.1021/ac2016823.

Giesen, C., Waentig, L., Panne, U., Jakubowski, N., 2012. History of inductively coupled plasma mass spectrometry-based immunoassays. Spectrochim. Acta - Part B At. Spectrosc. 76, 27–39. https://doi.org/10.1016/j.sab.2012.06.009.

Giesen, C., Wang, H.A.O., Schapiro, D., Zivanovic, N., Jacobs, A., Hattendorf, B., Schüffler, P.J., Grolimund, D., Buhmann, J.M., Brandt, S., Varga, Z., Wild, P.J., Günther, D., Bodenmiller, B., 2014. Highly multiplexed imaging of tumor tissues with subcellular resolution by mass cytometry. Nat. Methods 11, 417–422. https://doi.org/10.1038/nmeth.2869.

Grossman, H.B., Liebert, M., Antelo, M., Dinney, C.P., Hu, S.X., Palmer, J.L., Benedict, W.F., 1998. p53 and RB expression predict progression in T1 bladder cancer. Clin. Cancer Res. 4, 829–834.

Hoesl, S., Neumann, B., Techritz, S., Linscheid, M., Theuring, F., Scheler, C., Jakubowski, N., Mueller, L., 2014. Development of a calibration and standardization procedure for LA-ICP-MS using a conventional ink-jet printer for quantification of proteins in electro- and Western-blot assays. J. Anal. At. Spectrom. 29, 1282–1291. https://doi.org/10.1039/c4ja00060a.

Hoesl, S., Neumann, B., Techritz, S., Sauter, G., Simon, R., Schlüter, H.W., Linscheid, M., Theuring, F., Jakubowski, N., Mueller, L., 2016. Internal standardization of LA-ICP-MS immuno imaging via printing of universal metal spiked inks onto tissue sections. J. Anal. At. Spectrom. 31, 801–808. https://doi.org/10.1039/c5ja00409h.

Konz, I., Fernández, B., Fernández, M.L., Pereiro, R., Sanz-Medel, A., 2012. Laser ablation ICP-MS for quantitative biomedical applications. Anal. Bioanal. Chem. 403, 2113–2125. https://doi.org/10.1007/s00216-012-6023-6.

Krause, M., Scheler, C., Bottger, U., Weisshoff, H., Linscheid, M.W., 2002. Method and Reagent for Specifically Identifying and Quantifying One or More Proteins in a Sample.

Lou, X., Zhang, G., Herrera, I., Kinach, R., Ornatsky, O., Baranov, V., Nitz, M., Winnik, M.A., 2007. Polymer-based elemental tags for sensitive bioassays. Angew. Chemie - Int. Ed. 46, 6111–6114. https://doi.org/10.1002/anie.200700796.

McDevitt, M.R., Ma, D., Simon, J., Frank, R.K., Scheinberg, D.A., 2002. Design and synthesis of225Ac radioimmunopharmaceuticals. Appl. Radiat. Isot. 57, 841–847. https://doi.org/10.1016/S0969-8043(02)00167-7.

Moraleja, I., Esteban-Fernández, D., Lázaro, A., Humanes, B., Neumann, B., Tejedor, A., Mena, M.L., Jakubowski, N., Gómez-Gómez, M.M., 2016. Printing metal-spiked inks for LA-ICP-MS bioimaging internal standardization: comparison of the different nephrotoxic behavior of cisplatin, carboplatin, and oxaliplatin. Anal. Bioanal. Chem. 408, 2309–2318. https://doi.org/10.1007/s00216-016-9327-0.

Moraleja, I., Mena, M.L., Lázaro, A., Neumann, B., Tejedor, A., Jakubowski, N., Gómez-Gómez, M.M., Esteban-Fernández, D., 2018. An approach for quantification of platinum distribution in tissues by LA-ICP-MS imaging using isotope dilution analysis. Talanta 178, 166–171. https://doi.org/10.1016/j.talanta.2017.09.031.

Nieto, M., Gil-Bea, F.J., Dalfó, E., Cuadrado, M., Cabodevilla, F., Sánchez, B., Catena, S., Sesma, T., Ribé, E., Ferrer, I., Ramírez, M.J., Gómez-Isla, T., 2006. Increased sensitivity to MPTP in human α-synuclein A30P transgenic mice. Neurobiol. Aging 27, 848–856. https://doi.org/10.1016/j.neurobiolaging.2005.04.010.

Paxinos, G., Franklin, K.B.J., 2008. The Mouse Brain in Stereotaxic Coordinates, 3rd edn. Elsevier Academic Press, New York.

Schwarz, G., Mueller, L., Beck, S., Linscheid, M.W., 2014. DOTA based metal labels for protein quantification: a review. J. Anal. At. Spectrom. 29, 221–233. https://doi.org/10.1039/c3ja50277e.

Seuma, J., Bunch, J., Cox, A., McLeod, C., Bell, J., Murray, C., 2008. Combination of immunohistochemistry and laser ablation ICP mass spectrometry for imaging of cancer biomarkers. Proteomics 8, 3775–3784. https://doi.org/10.1002/pmic.

200800167.
Waentig, L., Jakubowski, N., Hardt, S., Scheler, C., Roos, P.H., Linscheid, M.W., 2012. Comparison of different chelates for lanthanide labeling of antibodies and application in a Western blot immunoassay combined with detection by laser ablation (LA-)ICP-MS. J. Anal. At. Spectrom. 27, 1311. https://doi.org/10.1039/c2ja30068k.
Wang, H.A.O., Grolimund, D., Giesen, C., Borca, C.N., Shaw-Stewart, J.R.H., Bodenmiller, B., Günther, D., 2013. Fast chemical imaging at high spatial resolution by laser ablation inductively coupled plasma mass spectrometry. Anal. Chem. 85, 10107–10116. https://doi.org/10.1021/ac400996x.
Whetstone, P.A., Butlin, N.G., Corneillie, T.M., Meares, C.F., 2004. Element-coded affinity tags for peptides and proteins. Bioconjug. Chem. 15, 3–6. https://doi.org/10.1021/bc034150l.
Yalow, R.S., Berson, S.A., 1996. Immunoassay of endogenous plasma insulin in man. Obes. Res. 4, 583–600. https://doi.org/10.1002/j.1550-8528.1996.tb00274.x.